# Journal of Materials Chemistry A

Accepted Manuscript


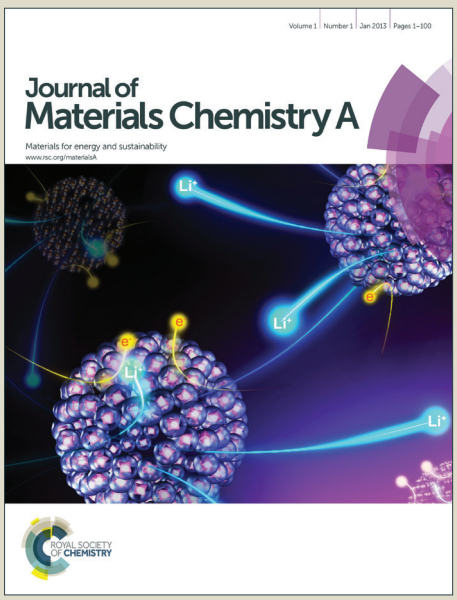





ROYAL SOCIETY OF CHEMISTRY

www.rsc.org/materialsA

Journal Name

RSCPublishing

ARTICLE

# Novel sulfonated polyimide/polyvinyl alcohol blend membranes for vanadium redox flow battery applications

Cite this: DOI: 10.1039/xoxxoooooox

Received ooth January 2012,
Accepted ooth January 2012

DOI: 10.1039/xoxxoooooox

www.rsc.org/

Shuai Liu,[a,b] Lihua Wang,[a*] Bin Zhang,[c] Biqian Liu,[a] Jianjun Wang,[a] and Yanlin Song[a]

The synthesis and characterization of novel sulfonated polyimide (SPI)/polyvinyl alcohol (PVA) blend membranes for the use in vanadium redox flow battery (VRB) are presented in this paper. The SPI with angled structure were synthesized using 4,4-oxydiphthalic anhydride (ODPA), sodium 2-aminosulphanilate(SAS) and 4,4'-diamino-3,3'-dimethyldiphenylmethane (DMMDA). The degree of sulfonation (DS) was regulated through variation of the molar ratio of SAS to the DMMDA. The PVA/SPI blend membranes were prepared and applied in VRB. Many basic properties of the membranes were characterized especially the water and oxidative stability. As a result, the blend membranes exhibit excellent water and oxidative stability. The proton conductivity, vanadium ion permeability and the proton selectivity increase with DS due to the highly-dispersed phase-separated microstructure. In VRB single cell tests, the VRBs with blend membranes show lower charge capacity loss, higher coulombic efficiency (CE) and energy efficiency (EE) than Nafion 117 membrane. Furthermore, the blend membranes present stable performance up to 100 cycles without significant decline in EE. All experimental results indicate that the blend membranes show promising prospects for VRB.

The vanadium redox flow battery (VRB) was pioneered by Skyllas-kazacos in 1985[1-3] and has attracted considerable attention as a large-scale energy storage system due to its high energy efficiency, long cycle life, fast response time and flexible design. Now the global demand for VRB is urgent, but its commercialization process is still heavily hindered by the relatively high cost of the key materials, especially the ion conducting membrane (ICM)[4]. In a VRB system, the ICM is one of the key materials, which effectively separates the anode and cathode electrolytes while allowing the transport of protons to complete the circuit. The ideal membranes used for VRB should exhibit high proton conductivity, low vanadium ions permeability, and possess high mechanical and chemical stability[5].

At present, the most widely used ICMs are Nafion series membranes (DuPont)[6, 7]. Even though the Nafion membranes show high chemical stability and proton conductivity, the high cost and vanadium ion permeability have limited the further commercialization of VRB[8, 9]. In addition, modification Nafion and modification polyvinylidene fluoride were also investigated and used in VRB[10-12]. These membranes exhibited lower vanadium ion permeability and good mechanical stability. However, the costs of these membranes are still higher as a result of the complex modification process[13]. In order to reduce the cost, massive efforts are engaged in developing substitute with low cost as well as excellent performance. In the past few decades, the most studied VRB membranes were non-fluorinated ion exchange membranes like sulfonated or quaternary ammoniated polyaromatic membranes, such as sulfonated poly(ether ether keton) (SPEEK), sulfonated polyimide (SPI), and sulfonated polysulfone (SPSF) due to their lower costs, outstanding mechanical and chemical stabilities[14-21].

Among them, SPI has been studied as ICM materials for its good mechanical property, low vanadium ions crossover, and thermal stability[14, 22-28]. Despite the above-mentioned salient properties, the hydrolytic stability is the primary obstacle in the application of VRB[29]. Various approaches have been put forward to develop membranes with higher hydrolytic stability. One method is to modify their structures based on the synthesis of polyimides with six-membered ring and use of novel sulfonated diamines with high basicity, linear configuration, and flexible linkages. However, polyimides with six-membered ring and novel sulfonated diamines are difficult to synthesize. Another strategy involves some crosslinking methods such as covalent crosslinking[30-32] and ionic crosslinking by introduction of polymeric bases[33, 34].

Detailed studies on cation exchange membranes proposed an essentially two-phase model [35-37] comprising a hydrophobic polymer backbone and hydrophilic ion exchange groups. Most water molecules are strongly localized near the hydrophilic zone. Hence, highly-dispersed phase-separated microstructure may be a viable option to improve the water stability of membranes while retaining the proton conductivity.

To fulfill this demand, polyvinyl alcohol (PVA) was introduced to blend with SPI. PVA have been widely studied as proton exchange membrane materials in the literature due to its good mechanical and chemical stability[38-43]. It can be industrially produced rather cheaply and can easily form large surface-area membranes. However, PVA does not have any negatively charged ions, rendering it a poor proton conductor. Therefore, an angled comonomer was introduced into the SPI[44, 45]. The angled comonomer forces the chains to separate and creates free volume between the polymer backbones which contribute to increasing proton conductivity.

In this paper, a series of novel SPI (Scheme 1) were synthesized with 4,4-oxydiphthalic anhydride (ODPA), 4,4'-diamino-3,3'-dimethyldiphenylmethane (DMMDA) and sodium 2-aminosulphanilate (SAS). PVA/SPI blend membranes were prepared in order to find new materials that have maximum proton selectivity and good water stability for VRB application. The microstructure and mechanical properties of the membranes were observed. Water uptake (WU), ion exchange capacity (IEC), proton conductivity and vanadium ion permeability were investigated. Oxidative stability and hydrolytic stability were studied in details. In the VRB single cell performance, 100 charge-discharge cycles were discussed and the corresponding coulombic, energy and voltage efficiencies were also obtained.

Scheme 1 Synthesis of sulfonated polyimide.

## Experimental

### Materials

ODPA was purchased from Shanghai Research Institute of synthetic resins and purified by vacuo sublimation prior to use. SAS and DMMDA were obtained from Chengdu Mixcy Reagent co. Ltd. DMMDA and SAS were dried in vacuum at 60 °C for 24 hours before used.

Nafion 117 membrane was purchased from DuPont Co. PVA ($M_w$= 74 800, degree of hydrolysis of 99%) was provided from Shanxi Sanwei Group co. Ltd. and used as received. Carbon felt and graphite felt were purchased from Beijing Jixing sheng'an Industry&Trade Co. Ltd., 99.999%; Dimethylformamide (DMF), triethylamine ($Et_3N$), acetic anhydride, dimethyl sulfoxide (DMSO), NaCl, NaOH, $MgSO_4$ and $H_2SO_4$ were obtained from Beijing chemical reagent co. Ltd. DMF and $Et_3N$ were purified by distillation under reduced pressure and dehydrated with 4 Å molecular sieves prior to use. Other reagents were used as received without further purification. All water was deionized.

### Synthetic procedures

SPI was prepared by the conventional two-step polymerization method involving ring-opening polyaddition forming poly(amic acid) and subsequent chemical imidization.

Typical procedure for the polyaddition of SPI is described as follows. DMMDA (1.130 g, 5mmol), SAS (1.051 g, 5mmol) were dissolved in DMF (35 ml) with stirring under nitrogen flow at ice-bath. After diamines were completely dissolved, ODPA (3.1021 g, 10mmol) was added to the solution in one portion. Thus, the solid content of the solution was approximately 14 wt.%. The solution was stirred at ice-bath for 16 h to yield a viscous polyamic acid solution. The precursor polyamic acid was subsequently chemically cyclized in solution to give the polyimide. A mixture of acetic anhydride (3 g) and $Et_3N$ (3 g) were added into the preceding polyamic acid solution and the reaction mixture was stirred at room temperature for 20 h. Finally, the solution mixture was poured into acetone. The fiber-like precipitate was washed with acetone several times and dried under vacuum at 80 °C for 24 h. In this study, the SPI obtained from ODPA, DMMDA and SAS will be referred to OMS. The degree of sulfonation (DS) was controlled by adjusting the molar ratio of SAS and DMMDA. The polyimides prepared with four different molar ratios and are named in numbers reflect the ratio of SAS/DMMDA: 40/60 (OMS-4), 50/50 (OMS-5), 60/40 (OMS-6), and 70/30 (OMS-7).

### Preparation of PVA/OMS blend membranes

The PVA/OMS blend membranes were prepared using solution casting method. 1 g PVA and 1 g OMS were dissolved in 12 g DMSO at 80 °C. After cooled to room temperature, the mixture solution was placed onto a flat glass, evaporated under infrared lamp, and then dried at 80 °C under vacuum for 12 h. The fabricated PVA/OMS blend membrane was peeled off from the glass, soaked in 3.6 wt.% formaldehyde in 25 wt.% $H_2SO_4$ solution for 3 h to carry out the crosslinking reaction. The resulting membrane was in the triethylamine salt form and was converted to the proton form by treating it with 1 mol $L^{-1}$ hydrochloric acid solution for 48 h and kept in deionized water before using. The thickness of the blend membrane is about 58-68 μm.

### Characterization of OMS

$^1$H NMR spectra were recorded on a Bruker DRX 300 MHz instrument using DMSO-$d_6$ as solvent. The thermal behaviours of the copolymers were measured on a TA instruments TGA 2050. The samples were evaluation from 30 °C to 900 °C in nitrogen at a heating rate of 10 K/min.

### Characterization of PVA/OMS blend membranes

FT-IR spectra of the membranes were measured by Bruker TENSOR-27 in the range of 4000-600 $cm^{-1}$. The samples were dried at 80 °C for 12 h before measurements. The morphology of the blend membranes were examined with SEM (Hitachi S4800). All the samples for cross-sectional view were fracture in liquid nitrogen. The crystal structures of blend membranes were examined using XRD (D/Max-2500, Rigaku Co., Japan) for 2θ angles between 5° and 50°. The mechanical properties of the blend membranes were measured by a tensile machine (Instron 5567, TA Instruments Co.) at elongation rate of 5.0 mm $min^{-1}$. All membranes were tested five times to obtain an average value.

The membranes were weighed after being dried under vacuum at 80 °C for 24 h. Subsequently, the membranes were immersed in deionized water for 24 h at room temperature. After quickly wiping off the water adhered to the surface, the weights of wet membranes were measured. The WU could be determined according to the following equations:

$$water\ uptake = \frac{W_{wet} - W_{dry}}{W_{dry}} \times 100\% \quad (1)$$

Where $W_{wet}$ and $W_{dry}$ are the weights of membranes in wet and dry state, respectively.

The IEC was obtained by titration method. The dry membranes were immersed in the 1mol $L^{-1}$ NaCl solution for 24 h. This solution was titrated by 0.01 mol $L^{-1}$ NaOH with phenolphthalein as the indicator. The IEC of the samples was calculated by following equation:

$$IEC = \frac{V_{NaOH} C_{NaOH}}{W_d} \quad (2)$$

Where $V_{NaOH}$ is the volume of consumed NaOH solution, $C_{NaOH}$ is the concentration of NaOH solution and $W_d$ is the weight of the dry membrane. All membranes were tested five times to obtain an average value.

The theoretical IEC can be calculated according to the DS by following equation:

$$IEC = \frac{DS}{2(500.5 - 38.1DS)} \quad (3)$$

The area resistance of the membrane was measured by the method as described in literature[12]. The measurement was performed with a bi-compartmental device which consists of two cells separated by the membrane. Both compartments were filled with 1 mol $L^{-1}$ $H_2SO_4$. The effective area of the membrane was 0.785 $cm^2$. The electric resistance was measured by electrochemical impedance spectroscopy (EIS) (Zahner Zennium) over a frequency range from 100 kHz to 100 MHz. The resistance value associated with the membrane conductance was determined from a high-frequency intercept of the impedance with the real axis. The area resistance can be calculated by the following expressions and all membranes were tested three times to obtain an average value

$$R = (r_1 - r_2)S \quad (4)$$

Where $r_1$ and $r_2$ represent the resistances of the cell with and without the membrane respectively.

The proton conductivity ( $\delta$ ) was calculated using the equation:

$$\delta = L / R \quad (5)$$

Where $L$ and $R$ were the thickness and area resistance of the membrane, respectively.

To measure the vanadium ions permeability, the membranes were exposed into a solution of 1.5 mol $L^{-1}$ $VOSO_4$ and 3 mol $L^{-1}$ $H_2SO_4$ (120 mL the left reservoir) and a solution of 1.5 mol $L^{-1}$ $MgSO_4$ and 3 mol $L^{-1}$ $H_2SO_4$ (120 mL the right reservoir). $MgSO_4$ was used to equalize the ionic strengths and to reduce the osmotic pressure effect. The effective area of the membrane was 0.785 $cm^2$. Samples from the right reservoir were taken at a regular time interval and analyzed for vanadium ions concentration by using an UV-vis spectrometer (UV-2550, SHIMADZU). The vanadium ions permeability was calculated by the following equation:

$$V_R \frac{dc_R(t)}{dt} = A\frac{P}{l}\left[c_L - c_R(t)\right] \quad (6)$$

Where $P$ was the vanadium ion permeability, $C_L$ was the vanadium ion concentration in the left reservoir, and $C_R$(t) was the vanadium ion concentration in the right reservoir as a function of time. $A$ and $l$ were the area and thickness of the membrane, respectively. $V_R$ was the volume of right reservoir. It is supposed the change of vanadium ion concentration in the left reservoir can always be negligible.

As illustrated in the literature[15, 46], the oxidative stability of the membrane was evaluated according to the ex-situ method. A sample of each membrane (25 mm×25 mm) was soaked in 25 mL of 0.15 mol $L^{-1}$ V(V) in 3.0 mol $L^{-1}$ $H_2SO_4$ obtained by diluting the fully charged positive half-cell electrolyte. V(IV) ions concentration was recorded as an indicator to measure the degree of oxidation of the membrane. Samples were taken at a regular time interval and analysed for vanadium ions concentration by an UV-vis spectrometer (UV-2550, SHIMADZU). All membranes were tested three times to obtain an average value.

The hydrolytic stability test was performed by immersing the membranes into deionized water at 60 °C (PVA could dissolve in water at 80 °C). The criterion for the judgment of the loss of mechanical properties is that the membrane is broken when lightly bent[47]. All membranes were tested three times to obtain an average value.

### VRB single cell performance

A VRB single cell was manufactured by sandwiching the membrane between two pieces of graphite felt electrodes with effective reaction area of 30×30 $mm^2$. The current collector material was graphite plate. The solutions of 1.5 mol $L^{-1}$ $V^{3+}$ in 3.0 mol $L^{-1}$ $H_2SO_4$ and 1.5 mol $L^{-1}$ $VO^{2+}$ in 3.0 mol $L^{-1}$ $H_2SO_4$ were served as initial negative and positive electrolyte, respectively. The volume of electrolyte on each side of the cell was 90 mL. Both the positive electrolyte and negative electrolyte were cyclically pumped into the corresponding half-cell at 5 L $min^{-1}$. Charge-discharge cycling test was conducted by LAND CT2001A with a constant current density of 30 mA $cm^{-2}$ at 25 °C. To avoid the corrosion of graphite felt, the cut-off voltage for charge and discharge was set as 1.65 V and 0.8 V respectively to avoid the corrosion of graphite felts and graphite plates.

The coulombic efficiency (CE), voltage efficiency (VE), and energy efficiency (EE) of the cell are calculated as following equations

$$CE = \frac{Q_{dis}}{Q_{ch}} \times 100\% = \frac{I_{ch} t_{dis}}{I_{ch} t_{ch}} \times 100\% = \frac{t_{dis}}{t_{ch}} \times 100\% \quad (7)$$

$$VE = \frac{V_{dis}}{V_{ch}} \times 100\% \quad (8)$$

$$EE = CE \times VE \quad (9)$$

## Results and discussion

### Characterization of sulfonated polyimide

Fig. 1. $^1$H-NMR spectrum of OMS-4 in DMSO-$d_6$.

The chemical structure of the obtained product was characterized by $^1$H NMR spectra. $^1$H NMR spectrum of OMS-4 is shown in Fig. 1. DS is calculated from integral ratio of H1 to H4. The molar ratio of SAS/DMMDA and the DS are shown in Table 1.

Fig. 2. TGA curves for OMS with different DS.

The thermal stability of OMS was measured by TGA in nitrogen and the related curves are shown in Fig. 2. The OMS

has three-step degradation pattern. The first step is observed around 100 °C, which is attributed to the loss of absorbed moisture by the highly hydrophilic sulfonic acid groups. The second step is observed within 220-400 °C which is attributed to the decomposition of sulfonic acid groups. Obviously, the amount of weight lost in this step varied directly with the DS. The third step about 500 °C corresponds to the decomposition of the polymer main chains. The TGA curves clearly indicate that this type of SPI has fairly good thermal stability.

**Characterization of PVA/OMS blend membranes**

Fig. 3. FT-IR spectra of PVA/OMS blend membranes

FT-IR spectra of PVA/OMS blend membranes are shown in Fig. 3. As for the membranes, the characteristic absorption bands at 1780 $cm^{-1}$ (C=O, asymmetric stretching), 1720 $cm^{-1}$ (C=O, symmetric stretching), 1380 $cm^{-1}$ (C-N-C, stretching vibration) and 748 $cm^{-1}$ (C=O, bending vibrations) suggest the formation of imide structure. The characteristic absorption bands at 1068 $cm^{-1}$ and 1017 $cm^{-1}$ (S=O stretching) indicate the presence of sulfonic acid groups and increase with the relative amount of SAS. This is confirmed that the sulfonic acid groups are successfully introduced to the resulting polymer.

Fig. 4. SEM images of PVA/OMS blend membranes: (a-d) cross-section morphology; (e-h) surface morphology. Scale bar is 1 μm.

The microstructure could influence the properties of membranes. SEM was performed to investigate the structure of the PVA/OMS blend membranes. The images of cross-section and surface morphology of membranes are shown in Fig. 4. Just as expected, the blend membranes exhibit phase-separated microstructure distinctly. The cross-section images(a-d) display the microphase separated microstructure become clear with the increase of DS and the surface images(e-h) reveal the formation of irregularly circular domains (>2 μm) of PVA/OMS-4 and changed to regularly circular domains (~0.35 μm) of PVA/OMS-7.

This finding reveals that inferior miscibility of different main chains facilitates highly-dispersed microphase separation structure in blend membranes. The improved proton selectivity and water stability could benefit from this specific structure.

Fig. 5. XRD patterns of PVA/OMS membranes

In order to further investigate the structure of the blend membranes. XRD analyses of membranes were conducted and the patterns of blend membranes are presented in Fig. 5. It can be seen that PVA/OMS-4 membrane exhibits the peak at about 2θ=20º corresponding to the (101) plane of the crystalline PVA backbone and the peak intensity gradually decreased with the increase of sulfonic acid groups. This results show that even immersed in formaldehyde to carry out the cross-linking reaction, there still remains some crystalline structure in PVA/OMS-4. However, the crystallinity of PVA remarkably reduces with the increase of DS. In PVA/OMS-4 membrane, the phase-separated structures are more bulky than in other membranes which results in the formation of crystalline structure. It implies that highly-dispersed phase-separated structure intensified as the DS increased.

Fig. 6 The mechanical properties of different PVA/OMS blend membranes

The mechanical strength of the blend membrane is significant for VRB application to assure its stability as the electrolyte passes across the membrane. The blend membranes had been immersed in water for 21 days before measurement.

As shown in Fig. 6, the mechanical properties of blend membranes could improve with the increase of DS. Such enhancement in tensile strength and the elongation at break is mainly due to the fine dispersion of OMS in the blend membranes which leads less tress convergence during the elongation process. The above results indicate that the membranes are strong and tough enough to be used in VRB.

Table 1 Basic properties of PVA/OMS blend membranes and Nafion 117 membrane.

Fig. 7. WU and IEC of PVA/OMS blend membranes and Nafion 117 membrane.

Many significant properties, such as proton conductivity and WU are related to IEC. IEC directly depends on the content of free sulfonic acid groups in the membrane. From Fig. 7, it can be seen that IEC of the blend membranes generally increases with the DS and a little lower than Nafion 117. In addition, compared with theoretical IEC, the experimental IEC values of the blend membranes are much lower which probably due to the incomplete ionic exchange in the process of IEC measurement. Such a phenomenon has been observed with many other ionomer membranes[25, 48].

WU is another important parameter for ICM. It has an influence on the proton conductivity and water stability. The WUs of PVA/OMS membranes are also plotted in Fig. 7. With increase of IEC, the WUs increase in a linear fashion. It is because the area of hydrophilic domains increased with the DS.

Fig. 8. Concentration of vanadium ion with PVA/OMS blend membranes and Nafion117 membrane.

The concentration of vanadium ion as a function of time is depicted in Fig. 8, and the calculated vanadium permeability coefficients are illustrated in Table 1. All the blend membranes have lower permeability than that of Nafion 117 membrane. Even the WU of PVA/OMS-7 membrane is much higher than Nafion 117, the permeability of the PVA/OMS-7 membrane is only $13.52\times10^{-9}$ $cm^2$ $s^{-1}$ compared to $30.98\times10^{-9}$ $cm^2$ $s^{-1}$ of Nafion 117. Generally speaking, high WU can improve the proton conductivity while leads to high vanadium permeability. However, in PVA/OMS blend membranes, the existence of highly-dispersed domains which restrain vanadium ions crossover.

Fig. 9. The proton conductivity and proton selectivity of the PVA/OMS blend membranes and Nafion117 membrane.

Besides, proton conductivity is the most important performance of membranes and affected by many factors such as IEC, WU and microstructure. The proton conductivity of the blend membrane is presented in Fig. 9. As IEC and WU shown above, the proton conductivities exhibit a similar trend. And the proton conductivity of PVA/OMS-7 membrane (0.069 S $cm^{-1}$) is very close to that of Nafion 117 (0.079 S $cm^{-1}$), which can meet requirements of VRB.

To obtain better VRB single cell performance, the membranes should possess balance between proton conductivity and vanadium ion permeability. Therefore, proton selectivity defined as the ratio of proton conductivity to $VO^{2+}$ permeability coefficient is discussed in Fig. 9. The proton selectivity is effectively improved with the increase of DS. The PVA/OMS-6 and PVA/OMS-7 membrane show similar proton selectivity which is over two times of that of Nafion 117. Two reasons might cause such results. One is the increase of WU, IEC and the content of angled structure promotes the proton conductivity. The other is ascribed to the enhanced highly-dispersed hydrophilic domains restrain vanadium ions permeability.

**Membranes stability toward water and oxidation**

Sulfonated polyimides are vulnerable to hydrolytic degradation. It is a severe problem in commercialization of these membranes despite many advantages. To evaluate the water stability, PVA/OMS blend membranes were immersed into water at 60 °C [47]. All tested membranes maintained mechanical strength and no apparently change in appearance, flexibility, and toughness after being soaked in hot water for more than 500 h. The blend membranes exhibit better water stability than normal SPI with five-numbered ring. High WU will promote the hydrolytic degradation[49]. However, compared to OMS chains, the PVA chains are more hydrophilic. Most of water molecules are strongly localized near the PVA chains and only a few are attracted by the sulfonic groups due to the strong hydrogen bonding. Hence, as the aggregation of OMS chains, the hydrophilic PVA chains and the aggregation of OMS chains prevent imide rings from water molecules to decrease the hydrolytic degradation.

Fig. 10. Oxidative stability of PVA/OMS-7 membrane and Nafion 117.

The electrolytes used in the VRB contain strong oxidative pentavalent vanadium ion ($VO_2^+$). Therefore, the blend membranes should have excellent oxidative stability. In order to investigate the chemical stability, the membranes were immersed in 0.15 mol $L^{-1}$ V(V) solutions. The data are presented in Fig. 10. The concentration of $VO^{2+}$ slightly increased with time during experiment. Generally, compared to perfluorinated materials like Nafion, membranes made from hydrocarbon materials are less stable. Although the $VO^{2+}$ concentration in PVA/OMS-7 is little higher than Nafion 117, it is still at a very low level. The result shows the blend membranes have good oxidative stability and can meet the requirements for VRB application.

**VRB single cell performance**

Table 2 VRB single cell performance of Nafion117 and PVA/OMS blend membranes.

The VRB single cell performance with Nafion 117 and PVA/OMS blend membranes are summarized in Table 2. The charge-discharge tests were performed under the same current density of 30 mA $cm^{-2}$. The CE of single cell with all blend membranes is much higher than Nafion 117. In addition, the CE for blend membranes reduces slightly from 99.5% to 97.3% with the increase of DS. It is because the CE is determined by the vanadium ion permeability. All the blend membranes have much lower permeability than Nafion 117. Moreover, with the increase of DS, the proton conductivity increased much higher than vanadium ion permeability. So the highest proton selectivity was achieved with PVA/OMS-7 in VRB system. The cell employing PVA/OMS-7 shows a CE of 97.3% and a VE of 83.8%, which are slightly higher than the corresponding values of 92.3% and 83.2% for the cell employing Nafion 117. Hence, the energy efficiency of PVA/OMS-7 (81.51%) is found to be much higher than Nafion 117 (76.87%).

Fig. 11. Charge-discharge curves for VRB with Nafion 117 and PVA/OMS blend membranes.

The typical charge-discharge curves of VRB single cell with blend membranes and Nafion 117 are presented in Fig. 11. There is a capacity difference in the different systems. The cell capacity is controlled by area resistance, cycle time and vanadium ion permeability. The high area resistance leads to short cycle time. The capacity of VRB with blend membranes is lower than Nafion 117 except PVA/OMS-7. The discharge time of PVA/OMS-7 is slightly longer than Nafion 117 implied the higher EE.

Fig. 12. The self-discharge of the VRB with Nafion 117 and PVA/OMS-7 blend membrane.

Open circuit voltage (OCV) measurements are often used as an indirect method to investigate the self-discharge degree of VRB and reveal the transferring of the vanadium ions across the membranes. Fig. 12 displays the OCV of the VRB with Nafion 117 and PVA/OMS-7 blend membrane. It can be seen that the time of OCV beyond 0.8 V with PVA/OMS-7 blend membrane can last for more than 68 h, which is nearly 1.7 times longer than Nafion 117 under the same condition. The result demonstrates that the blend membranes have much lower vanadium ion permeability than Nafion 117.

Fig. 13. Cycling performance of VRB with PVA/OMS-7 blend membrane and Nafion 117.

To investigate the stability of PVA/OMS-7 membrane, the cyclic performance of single cells with PVA/OMS-7 membrane and Nafion 117 were carried at current density of 30 mA $cm^{-2}$. Fig. 13 shows that the single cell assembled with PVA/OMS-7 showed stable performance. The CE gradually increase to above 97% and the VE maintain beyond 80% after running for 100 cycles. It can be seen that the PVA/OMS-7 showed higher efficiencies than Nafion 117 indicating lower vanadium permeation rate, stable conductive channels and chemically stability in the VRB.

## Conclusions

A series of PVA/OMS blend membranes were prepared for VRB applications. The structures of the membranes were characterized by FT-IR, SEM and XRD. The results showed that the blend membranes exhibited micro-phase separation distinctly. The membrane properties such as mechanical properties, IEC, WU, water and oxidative stability, proton conductivity, and vanadium ion permeability were investigated. The blend membranes exhibited better water stability than normal SPI with five-membered ring due to the aggregation of hydrophilic PVA chains and hydrophobic OMS main chains. Compared to Nafion 117, the blend membranes obtained lower vanadium ion permeability and higher proton selectivity. In VRB single cell tests, the cells with blend membranes showed higher CE than Nafion 117 and the EE with PVA/OMS-7 membrane can reach 81.51%. The self-discharge rate of VRB with PVA/OMS-7 membrane was lower than Nafion 117. After 100 cycles, the PVA/OMS-7 membrane showed stably battery efficiency. Considering these results, PVA/OMS blend membranes are expected to be ideal membranes for VRB application.

## Acknowledgements

The authors express their thanks to the National Nature Science Foundation of China (No.21376253), National 973 Item (No.2009CB623407), Youth Innovation Promotion Association CAS, Center for Molecular Science (CMS-PY-201220) and K C. Wong Education Foundation Hong Kong for financial support.

## Notes and references

[a] Key laboratory of Green Printing, Institute of Chemistry, Chinese Academy of Sciences, Beijing, 100190, P.R. China.
[b] University of Chinese Academy of Sciences, 100049, P.R. China.
[c] School of materials science and engineering, Tianjin Polytechnic University, Tianjin, 300387, P. R. China.
† Corresponding author. Tel.: +86 10 6265 0812; Fax: +86 10 6255 9373.
E-mail: wanglh@iccas.ac.cn.

1. E. Sum and M. Skyllas-Kazacos, *J Appl Electrochem*, 1988, **18**, 731-738.
2. E. Sum and M. Skyllas-Kazacos, *J Power Sources*, 1985, **15**, 179-190.
3. E. Sum, M. Rychcik and M. Skyllas-Kazacos, *J Power Sources*, 1985, **16**, 85-95.
4. H. Z. Zhang, C. Ding, J. Y. Cao, W. X. Xu, X. F. Li and H. M. Zhang, *J Mater Chem A*, 2014, **2**, 9524-9531.
5. T. Mohammadi and M. Skyllas-Kazacos, *J. Membr. Sci.*, 1995, **107**, 35-45.
6. J. S. Lawton, D. S. Aaron, Z. J. Tang and T. A. Zawodzinski, *J. Membr. Sci.*, 2013, **428**, 38-45.
7. J. Y. Xi, Z. H. Wu, X. G. Teng, Y. T. Zhao, L. Q. Chen and X. P. Qiu, *J. Mater. Chem.*, 2008, **18**, 1232-1238.
8. T. Mohammadi, S. C. Chieng and M. Skyllas-Kazacos, *J. Membr. Sci.*, 1997, **133**, 151-159.
9. M. Skyllas-Kazacos, D. Kasherman, D. R. Hong and M. Kazacos, *J Power Sources*, 1991, **35**, 399-404.
10. J. Y. Qiu, J. Z. Zhang, J. H. Chen, J. Peng, L. Xu, M. L. Zhai, J. Q. Li and G. S. Wei, *J. Membr. Sci.*, 2009, **334**, 9-15.
11. X. G. Teng, Y. T. Zhao, J. Y. Xi, Z. H. Wu, X. P. Qiu and L. Q. Chen, *J. Membr. Sci.*, 2009, **341**, 149-154.
12. X. M. Yan, G. H. He, S. Gu, X. M. Wu, L. G. Du and H. Y. Zhang, *J. Membr. Sci.*, 2011, **375**, 204-211.
13. X. F. Li, H. M. Zhang, Z. S. Mai, H. Z. Zhang and I. Vankelecom, *Energ Environ Sci*, 2011, **4**, 1147-1160.
14. M. Z. Yue, Y. P. Zhang and L. Wang, *Solid State Ionics*, 2012, **217**, 6-12.
15. S. Winardi, S. C. Raghu, M. O. Oo, Q. Y. Yan, N. Wai, T. M. Lim and M. Skyllas-Kazacos, *J. Membr. Sci.*, 2014, **450**, 313-322.
16. W. X. Xu, X. F. Li, J. Y. Cao, H. Z. Zhang and H. M. Zhang, *Sci Rep-Uk*, 2014, **4**.
17. L. Semiz, N. D. Sankir and M. Sankir, *J. Membr. Sci.*, 2014, **468**, 209-215.
18. Z. H. Li, W. J. Dai, L. H. Yu, J. Y. Xi, X. P. Qiu and L. Q. Chen, *J Power Sources*, 2014, **257**, 221-229.
19. C. W. Hwang, H. M. Park, C. M. Oh, T. S. Hwang, J. Shim and C. S. Jin, *J. Membr. Sci.*, 2014, **468**, 98-106.
20. X. L. Wei, Z. M. Nie, Q. T. Luo, B. Li, B. W. Chen, K. Simmons, V. Sprenkle and W. Wang, *Adv. Energy Mater.*, 2013, **3**, 1215-1220.
21. S. H. Zhang, B. G. Zhang, G. F. Zhao and X. G. Jian, *J Mater Chem A*, 2014, **2**, 3083-3091.
22. L. Akbarian-Feizi, S. Mehdipour-Ataei and H. Yeganeh, *Int J Hydrogen Energ*, 2010, **35**, 9385-9397.
23. Y. Yin, J. H. Fang, Y. F. Cui, K. Tanaka, H. Kita and K. Okamoto, *Polymer*, 2003, **44**, 4509-4518.
24. Y. Yin, J. H. Fang, T. Watari, K. Tanaka, H. Kita and K. Okamoto, *J. Mater. Chem.*, 2004, **14**, 1062-1070.
25. W. Li, X. X. Guo and J. H. Fang, *J. Membr. Sci.*, 2014, **49**, 2745-2753.
26. J. C. Li, Y. P. Zhang and L. Wang, *J Solid State Electr*, 2014, **18**, 729-737.
27. Y. He, C. Y. Tong, L. Geng, L. D. Liu and C. Lu, *J. Membr. Sci.*, 2014, **458**, 36-46.
28. M. Z. Yue, Y. P. Zhang and L. Wang, *J Appl Polym Sci*, 2013, **127**, 4150-4159.
29. W. Jang, S. Sundar, S. Choi, Y. G. Shul and H. Han, *J. Membr. Sci.*, 2006, **280**, 321-329.
30. K. Miyatake, H. Zhou and M. Watanabe, *Macromolecules*, 2004, **37**, 4956-4960.
31. Y. Yin, S. Hayashi, O. Yamada, H. Kita and K. Okamoto, *Macromol. Rapid Comm.*, 2005, **26**, 696-700.
32. K. Vanherck, G. Koeckelberghs and I. F. J. Vankelecom, *Prog. Polym. Sci.*, 2013, **38**, 874-896.
33. J. A. Kerres, *Fuel Cells*, 2005, **5**, 230-247.
34. O. Savadogo, *J Power Sources*, 2004, **127**, 135-161.
35. K. D. Kreuer, S. J. Paddison, E. Spohr and M. Schuster, *Chem Rev*, 2004, **104**, 4637-4678.
36. B. J. Robbins, R. W. Field, S. T. Kolaczkowski and A. D. Lockett, *J. Membr. Sci.*, 1996, **118**, 101-110.
37. M. J. Park and S. Y. Kim, *J Polym Sci Pol Phys*, 2013, **51**, 481-493.

38. C. E. Tsai, C. W. Lin, J. Rick and B. J. Hwang, *J Power Sources*, 2011, **196**, 5470-5477.
39. T. Yang, *J. Membr. Sci.*, 2009, **342**, 221-226.
40. C. C. Yang, Y. J. Lee and J. M. Yang, *J Power Sources*, 2009, **188**, 30-37.
41. S. Gu, G. H. He, X. M. Wu, Y. J. Guo, H. J. Liu, L. Peng and G. K. Xiao, *J. Membr. Sci.*, 2008, **312**, 48-58.
42. A. K. Sahu, G. Selvarani, S. D. Bhat, S. Pitchumani, P. Sridhar, A. K. Shukla, N. Narayanan, A. Banerjee and N. Chandrakumar, *J. Membr. Sci.*, 2008, **319**, 298-305.
43. A. K. Sahu, G. Selvarani, S. Pitchumani, P. Sridhar, A. K. Shukla, N. Narayanan, A. Banerjee and N. Chandrakumar, *J Electrochem Soc*, 2008, **155**, B686-B695.
44. M. H. Litt, Y. Zhang, R. F. Savinell and J. S. Wainright, *Abstr Pap Am Chem S*, 1999, **218**, U560-U560.
45. H. J. Kim, M. H. Litt, S. Y. Nam and E. M. Shin, *Macromol Res*, 2003, **11**, 458-466.
46. D. J. Chen and X. F. Li, *J Power Sources*, 2014, **247**, 629-635.
47. J. H. Fang, X. X. Guo, S. Harada, T. Watari, K. Tanaka, H. Kita and K. Okamoto, *Macromolecules*, 2002, **35**, 9022-9028.
48. F. Zhang, N. W. Li, Z. M. Cui, S. B. Zhang and S. H. Li, *J. Membr. Sci.*, 2008, **314**, 24-32.
49. C. Genies, R. Mercier, B. Sillion, R. Petiaud, N. Cornet, G. Gebel and M. Pineri, *Polymer*, 2001, **42**, 5097-5105.

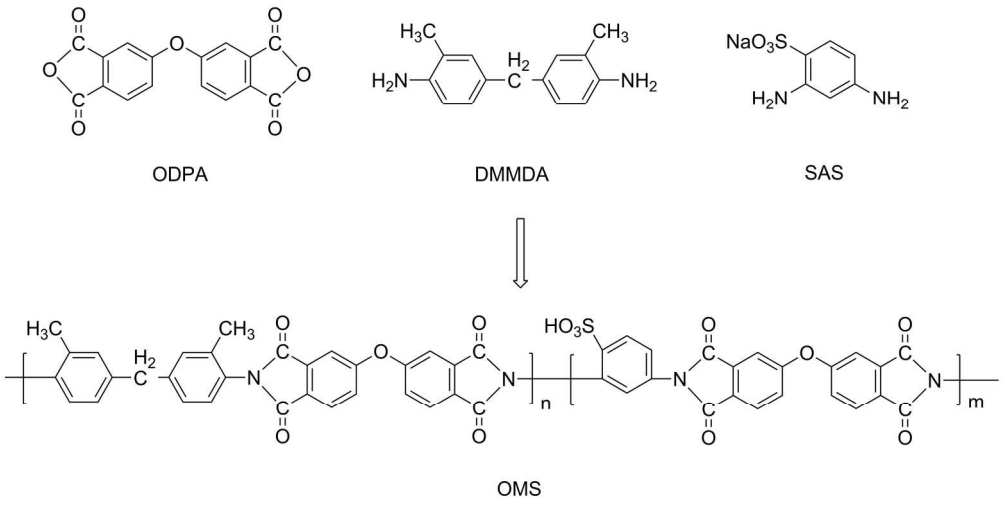


Synthesis of sulfonated polyimide.
89x44mm (600 x 600 DPI)

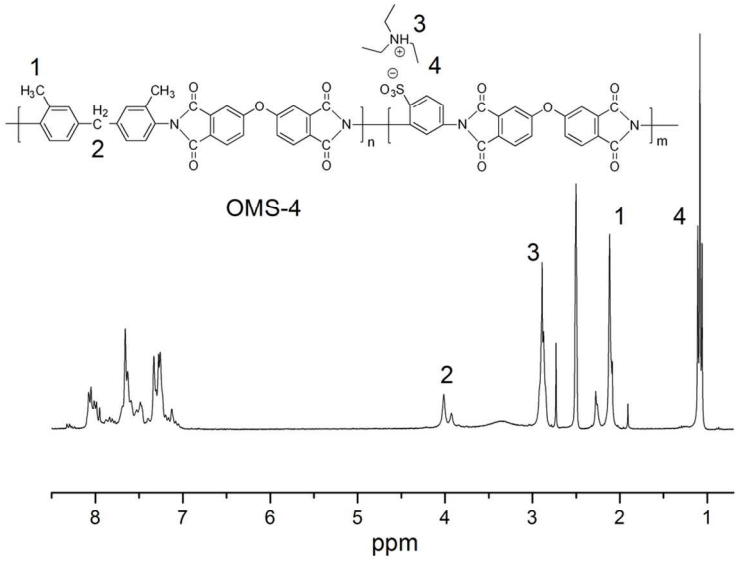


1H-NMR spectrum of OMS
58x41mm (600 x 600 DPI)

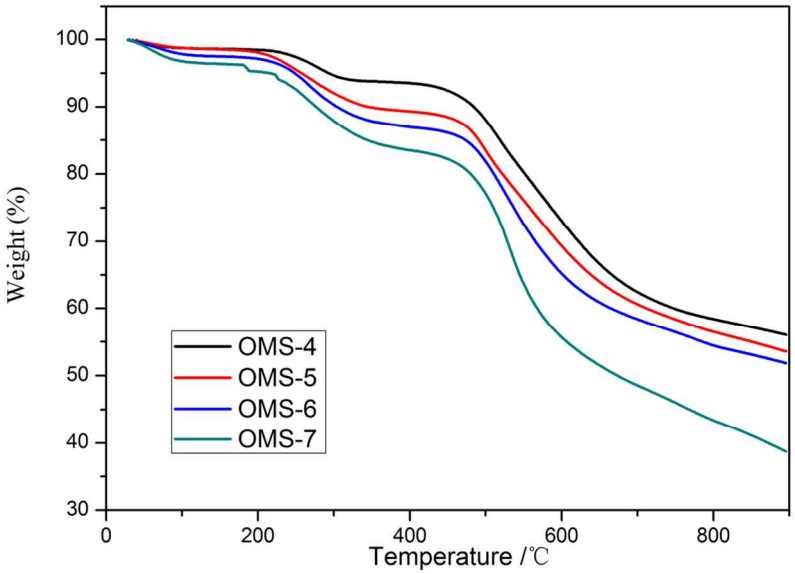


TGA curves for OMS with different DS.
58x40mm (600 x 600 DPI)

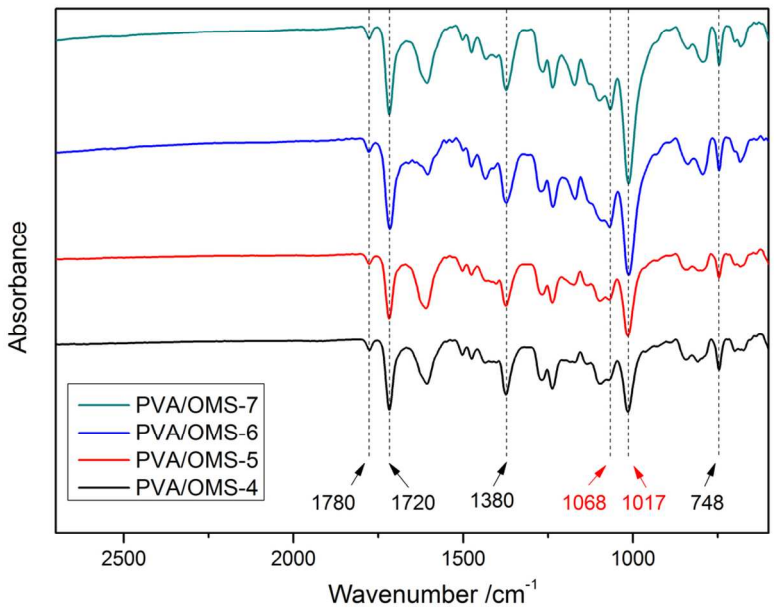


FT-IR spectra of PVA/OMS blend membranes
58x40mm (600 x 600 DPI)

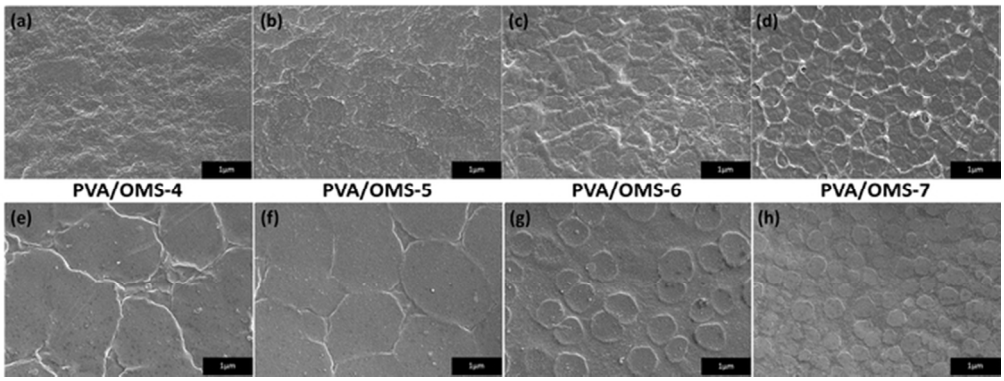


SEM images of PVA/OMS blend membranes: (a-d) cross-section morphology; (e-h) surface morphology. Scale bar is 1 μm.
59x22mm (300 x 300 DPI)

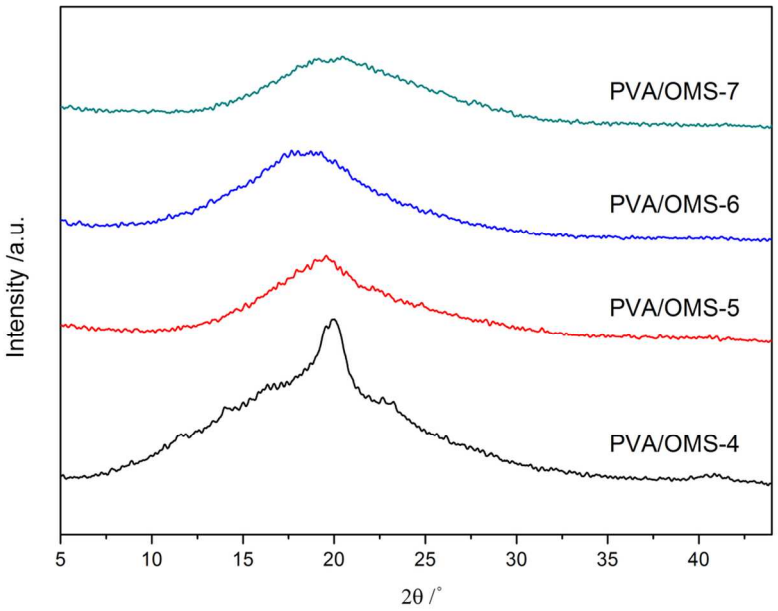


XRD patterns of PVA/OMS membranes
58x41mm (600 x 600 DPI)

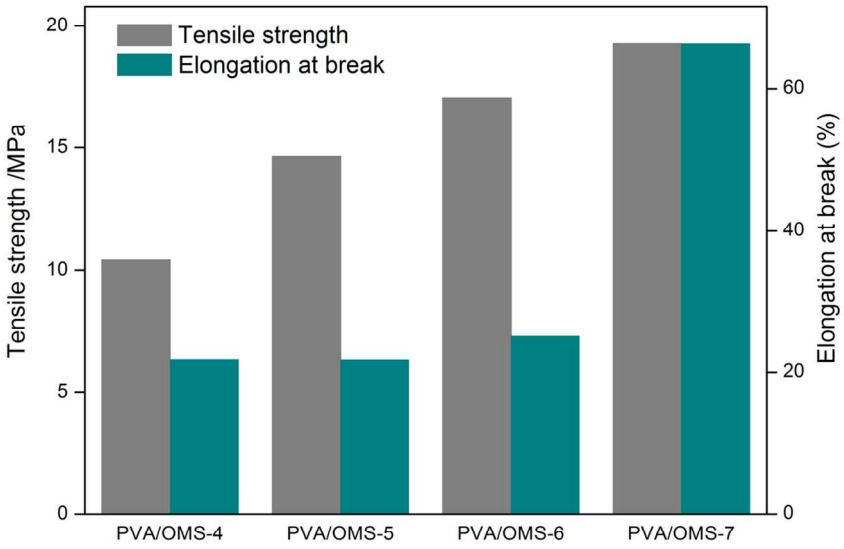


The mechanical properties of different PVA/OMS blend membranes
58x41mm (600 x 600 DPI)

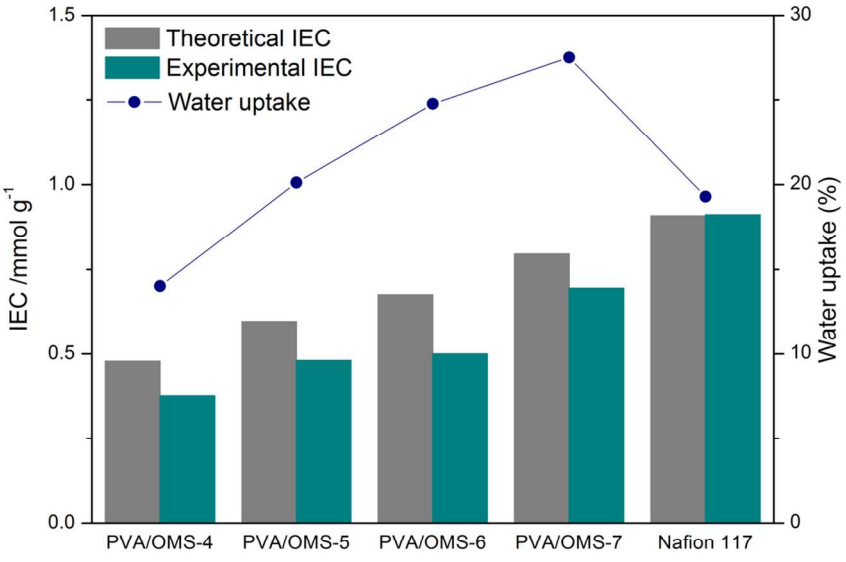


WU and IEC of PVA/OMS blend membranes and Nafion 117 membrane.

58x41mm (600 x 600 DPI)

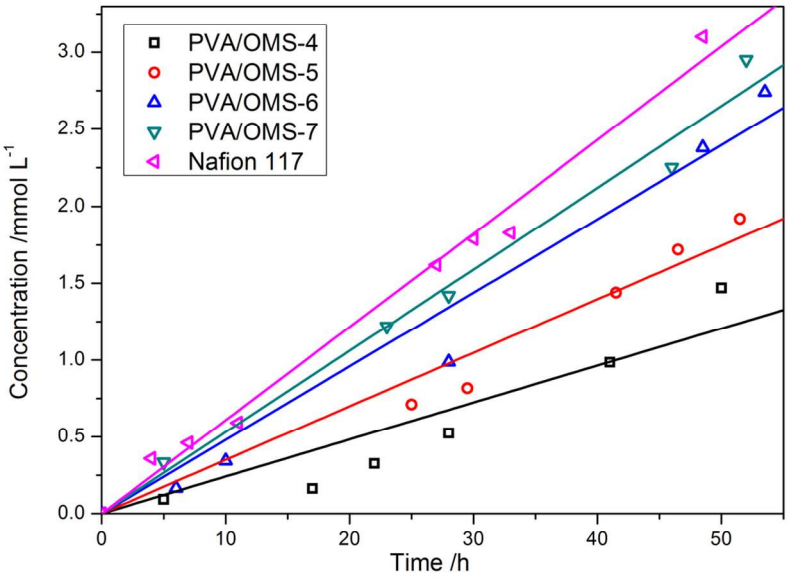


Concentration of vanadium ion with PVA/OMS blend membranes and Nafion117 membrane.
58x41mm (600 x 600 DPI)

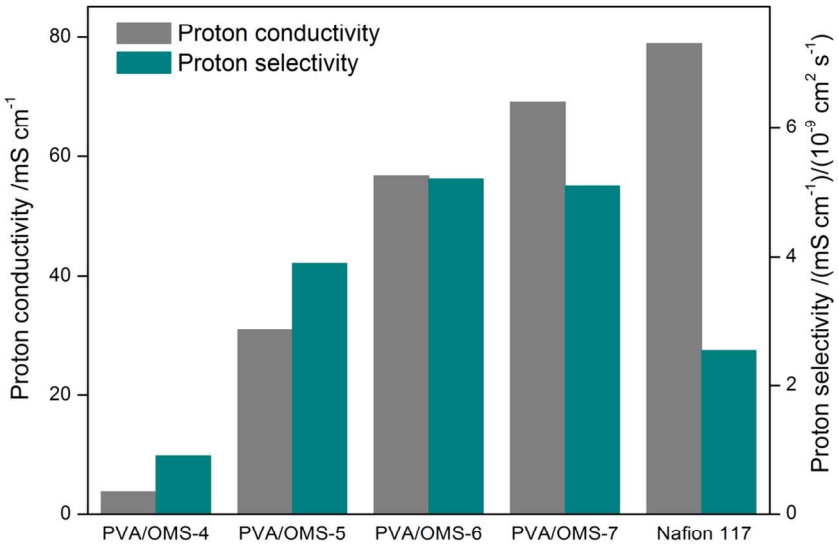


The proton conductivity and proton selectivity of the PVA/OMS blend membranes and Nafion117 membrane.
58x41mm (600 x 600 DPI)

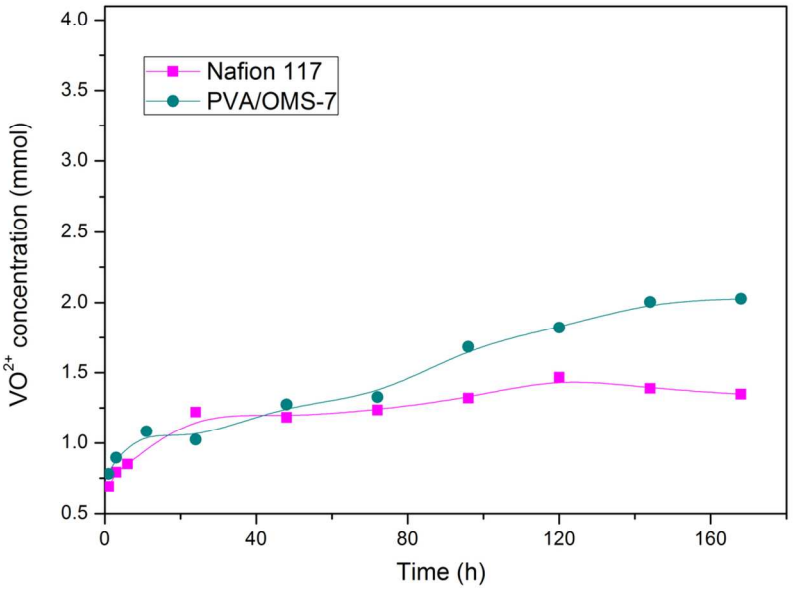


Oxidative stability of PVA/OMS-7 membrane and Nafion 117.
58x41mm (600 x 600 DPI)

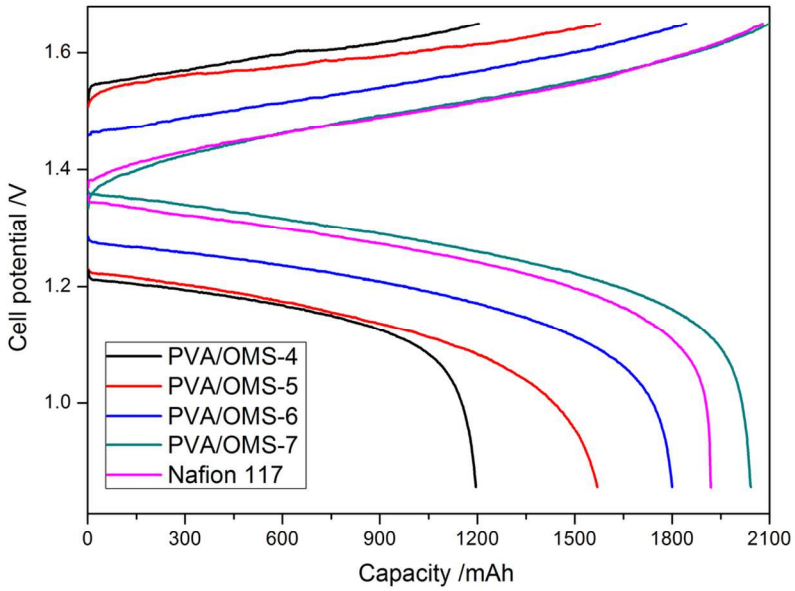


Charge-discharge curves for VRB with Nafion 117 and PVA/OMS blend membranes.
58x41mm (600 x 600 DPI)

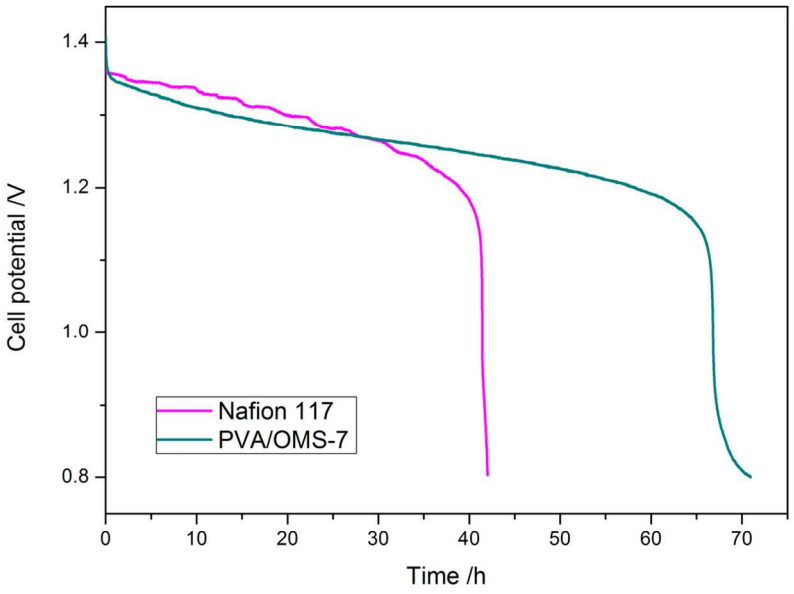


The self-discharge of the VRB with Nafion 117 and PVA/OMS-7 blend membrane.
58x41mm (600 x 600 DPI)

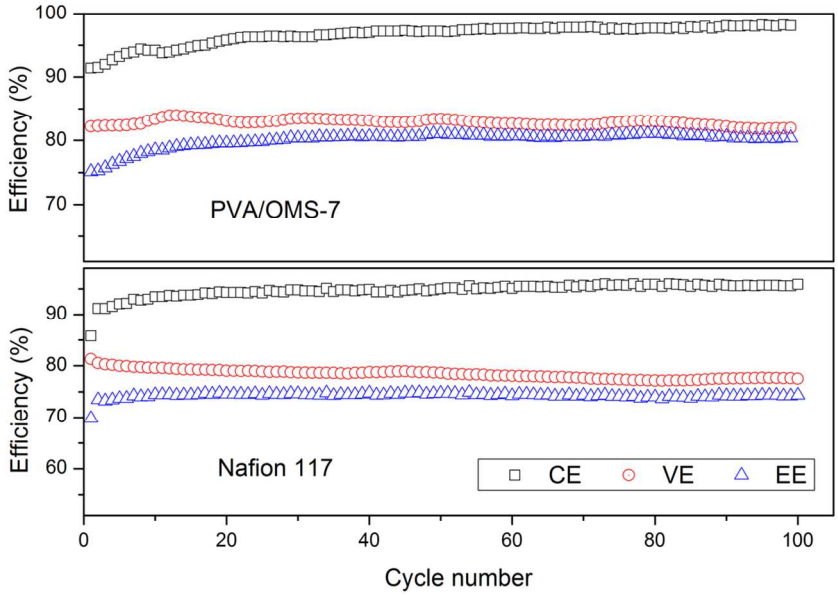


Cycling performance of VRB with PVA/OMS-7 blend membrane and Nafion 117.
58x41mm (600 x 600 DPI)

Table 1 Properties of PVA/OMS blend membranes and Nafion 117 membrane

| Membranes | SAS/DMMDA | DS (%) | WU (%) | IEC (mmol $g^{-1}$) | | Area resistance ($\Omega$ $cm^2$) | Proton conductivity (mS $cm^{-1}$) | $VO^{2+}$ permeability ($10^{-9}$ $cm^2$ $s^{-1}$) |
|---|---|---|---|---|---|---|---|---|
| | | | | Theoretical | Experimental | | | |
| PVA/OMS-4 | 40/60 | 46.2 | 14.02 | 0.478 | 0.376 | 1.758 | 3.697 | 4.10 |
| PVA/OMS-5 | 50/50 | 57.1 | 20.12 | 0.596 | 0.480 | 0.259 | 30.88 | 7.91 |
| PVA/OMS-6 | 60/40 | 64.3 | 24.77 | 0.675 | 0.500 | 0.141 | 56.77 | 10.88 |
| PVA/OMS-7 | 70/30 | 75.1 | 27.50 | 0.796 | 0.695 | 0.130 | 69.14 | 13.52 |
| Nafion 117 | N/A | N/A | 19.30 | 0.909 | 0.912 | 0.232 | 78.89 | 30.98 |

Table 2 VRB single cell performance of Nafion 117 and PVA/OMS blend membranes.

| Membranes | CE(%) | VE(%) | EE(%) |
|---|---|---|---|
| PVA/OMS-4 | 99.5 | 70.7 | 70.36 |
| PVA/OMS-5 | 98.9 | 72.3 | 71.53 |
| PVA/OMS-6 | 97.6 | 76.8 | 74.97 |
| PVA/OMS-7 | 97.3 | 83.8 | 81.51 |
| Nafion 117 | 92.3 | 83.2 | 76.87 |

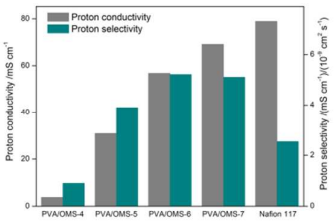


PVA/SPI blend membranes with highly highly-dispersed microphase separation structure for vanadium redox flow battery applications